Front. Struct. Civ. Eng. 2023, 17(3): 396–410
https://doi.org/10.1007/s11709-023-0934-5

RESEARCH ARTICLE

On braced trapezoidal corrugated steel shear panels: An experimental and numerical study

Vahid AMIRI, Arash AKBARI HAMED[*], Karim ABEDI

Faculty of Civil Engineering, Sahand University of Technology, Tabriz 5331817634, Iran
[*]Corresponding author. E-mail: akbarihamed.a@sut.ac.ir

ABSTRACT In this study, a new system consisting of a combination of braces and steel infill panels called the braced corrugated steel shear panel (BCSSP) is presented. To obtain the hysteretic behavior of the proposed system, the quasi-static cyclic performances of two experimental specimens were first evaluated. The finite element modeling method was then verified based on the obtained experimental results. Additional numerical evaluations were carried out to investigate the effects of different parameters on the system. Subsequently, a relationship was established to estimate the buckling shear strength of the system without considering residual stresses. The results obtained from the parametric study indicate that the corrugated steel shear panel (CSSP) with the specifications of a = 30 mm, t = 2 mm, and θ = 90° had the highest energy dissipation capacity and ultimate strength while the CSSP with the specifications of a = 30 mm, t = 2 mm, and θ = 30° had the highest initial stiffness. It can thus be concluded that the latter CSSP has the best structural performance and that increasing the number of corrugations, corrugation angle, and plate thickness and decreasing the sub-panel width generally enhance the performance of CSSPs in terms of the stability of their hysteretic behaviors.

KEYWORDS trapezoidal corrugated plate, steel shear panel, braced steel shear panel, experimental study, buckling resistance.

1 Introduction

The widespread damage of steel structures in the 1994 Northridge and 1995 Kobe earthquakes has resulted in extensive research on improving the performance of steel structures through various means such as the use of easily replaceable steel elements, self-centering steel structures, rocking steel structures, and smart materials [1]. Steel plate shear walls (SPSW) are common structural systems with acceptable performance against lateral forces in earthquake-prone areas. An SPSW comprises a steel infill panel and horizontal and vertical boundary members (beams and columns). The system behaves as a cantilevered vertical plate girder in which the columns and beams act as plate girder flanges and web stiffeners, respectively. This system has high initial elastic stiffness and ductility and an adequate capacity for seismic energy dissipation under earthquake loads. The most popular types of SPSW systems are unstiffened (simple) SPSWs and stiffened SPSWs. The limit states of unstiffened and stiffened SPSWs are tension field action development and shear yielding, respectively. The addition of stiffeners to simple shear panels to improve their efficiency by enhancing their buckling resistance has been suggested. The stiffeners contribute to a wider area in the infill panel for dissipating seismic energy through shear yielding and thereby increase the buckling resistance and ductility of the steel panels [2,3]. However, these two common types of SPSWs suffer from specific issues such as pinching of the cyclic force–displacement curve due to early buckling of the infill panel, the failure of boundary elements that are subjected to large distributed forces in unstiffened SPSWs, and the high cost of erecting stiffeners and possible low-cycle fatigue in the welding areas in stiffened SPSWs. Various solutions to address these issues have been suggested such as the use of half-bay SPSWs that are separated from columns [4,5], intermittent welding of SPSWs to boundary elements [6], perforated SPSWs [7–14], low-yield point materials [15–18], SPSWs with vertical slits [19], SPSWs with

Article history: Received Jul 11, 2022; Accepted Nov 22, 2022

tension bracing [20], braced steel shear panels [21–26], auxetic-shaped SPSWs [27] and optimized SPSWs [28].

One novel idea is the use of corrugated steel plate shear walls (CSPSWs), which were introduced by Berman [29]. Emami et al. [30] performed experimental studies on SPSWs with unstiffened and trapezoidal corrugated panels. The results show that the corrugated specimens had a higher seismic energy dissipation capacity, ductility ratio, and initial elastic stiffness than the unstiffened specimen. Yadollahi et al. [31] investigated the effects of various parameters on the structural performance of corrugated SPSWs. Hosseinpour et al. [32] studied the behavior of unstiffened and corrugated SPSWs with sinusoidal and trapezoidal patterns and demonstrated that trapezoidal plates had a higher capacity for seismic energy dissipation, ductility, and ultimate strength compared to sinusoidal plates. Farzampour et al. [33] conducted a parametric study on CSPSWs and unstiffened SPSWs with and without openings. They investigated the effects of critical parameters such as the plate thickness, corrugation angle, opening size, and opening placement and concluded that the lateral stiffness, seismic energy absorption, and ductility of trapezoidal CSPSWs were increased compared to those of unstiffened SPSWs. At the same time, the occurrence of ultimate strength was postponed but the ultimate strength was decreased. The structural performance of SPSWs with horizontal trapezoidal corrugations in which the center of the infill panel was perforated by square holes was investigated by Bahrebar et al. [34], who studied the effects of some plate parameters such as the corrugation angle, thickness, and opening size. The effects of various corrugation inclinations and their corresponding failure modes [35] along with different opening properties and infill panel thicknesses [36] on the seismic performance of CSPSWs were studied. Banazadeh and Maleki [37] investigated the behavior of SPSWs and demonstrated that the ductility and seismic energy absorption of corrugated systems were significantly increased compared with those of unstiffened systems. Dou et al. [38] studied the behavior of sinusoidal CSPSWs and presented an equation for estimating the shear buckling load with reasonable accuracy. Cao and Huang [39] numerically and experimentally investigated the hysteretic behavior of CSPSWs and concluded that appropriately designed CSPSW parameters can prevent elastic buckling and increase the initial elastic stiffness, strength, seismic energy absorption capacity, and ductility. Dou et al. [40] numerically studied the effects of initial geometrical imperfections and dimensions on the shear resistance of sinusoidally corrugated panels and proposed fitting relationships between the shear resistances of the panels and their normalized height-to-thickness ratios. Tong and Guo [41] numerically studied the shear strength of stiffened CSPSWs and concluded that out-of-plane deformations could be restrained by a stiffened plate and both the shear strength and ductility of stiffened CSPSWs could be enhanced. Feng et al. [42] used steel strips to stiffen CSPSWs and reduce the amount of out-of-plane deformation and proposed formulas for estimating their elastic buckling loads. A double CSPSW (DCSPSW) consisting of two bolted corrugated plates was proposed by Tong et al. [43–45]. They investigated its buckling behavior and concluded that this new type of CSPSW had more stable cyclic behavior compared to common CSPSWs. They also theoretically obtained the rigidity constants such as the flexural and torsional rigidities of the DCSPSWs. In addition, they presented validated equations for estimating the shear elastic buckling based on finite element (FE) analysis results and some design guidelines for designing DCPSWs. Ghodratian-Kashan and Maleki [46] conducted an experimental study on three half-scale DCSPSW specimens. The main results of this study were that detaching the infill panel from the columns reduced their axial forces and that specimens with attached or detached corrugated plates had similar structural performances. Bahrebar et al. [47] investigated the behavior of curved CSPSWs with centrally placed openings by using FE models to analyze the effects of geometrical parameters on the behavior of the models. The obtained results show that adequately designed curved CSPSWs with web perforations had desirable performance. Yu et al. [48] introduced a novel specially shaped CSPSW with composite elements. Based on the experimental observations, they concluded that this new system had high initial stiffness, ductility, and elastic shear strength.

In light of the acceptable structural performance of braced steel shear panels and CSPSWs that has been confirmed by various researchers, the aim of this study is to enhance the structural performance of braced steel shear panels by using corrugated steel shear panels (CSSPs) instead of stiffened and unstiffened panels. It should be mentioned that in braced shear panel systems, the shear panel is placed at the center of a story separately from the surrounding main beams and columns using the considered braces. This new system is expected to reduce the costs and other disadvantages of stiffened shear panels and address the pinching of the hysteretic curves of unstiffened shear panels. Two experimental specimens of this innovative type of SPSW, which is named the braced corrugated steel shear panel (BCSSP), were evaluated under the considered cyclic loading time history. After validating the accuracy of the considered FE modeling method with respect to the experimental results, a parametric study of the proposed system was performed to investigate the effects of some effective parameters such as the sub-panel width, corrugation angle, and panel thickness. Finally, a relationship to estimate the buckling shear strength of the system was established using surface regression.

2 Experimental study

2.1 Experimental setup and specimen details

In this study, two full-scale CSSP experimental specimens with the same sub-panel width (i.e., parameter a in Fig. 1) and various geometrical properties such as the number of ridges and grooves (i.e., corrugation) and corrugation angle were prepared and subjected to the considered quasi-static cyclic loading time history. The geometric properties of the considered specimens and the profile of the corrugated plates are shown in Table 1 and Fig. 1, respectively. As depicted in Fig. 1, the sub-panel width, corrugation angle, inclined part length, horizontal projection of the inclined part, corrugation height, and sub-panel width at the sides of the panel are denoted as a, θ, d, b, h, and c, respectively.

Figure 2(a) shows a schematic representation of a braced steel shear panel system in which the braces are connected to the boundary members using pinned connections. As shown in Fig. 2(b), the considered CSSP specimens contained boundary members with a double back-to-back UNP80 profile (i.e., a channel section), which were connected using pin connections at both ends. Along the direction parallel to the panel ridges and grooves, the corrugated plate was clamped between the boundary members using slip-critical high-strength bolted connections with a bolt diameter of 8 mm (Figs. 2(b) and 2(c)). The other two sides of the corrugated panels in the direction perpendicular to the panel ridges and grooves were connected to the surrounding members using L-shaped fish plates, welds, and rivets (Fig. 2(b)). Rivets and welds (i.e., hybrid joints) were used simultaneously to increase the safety factor of the plate at the connection and to prevent failure in the connection. The number of rivets required was determined based on the tensile capacity of the plate. To prepare the corrugated shear panels, flat plates were bent using an automatic machine. Figures 2(d), 2(e), and 2(f) show the geometrical dimensions and experimental setup of the CSSP specimens on a universal testing machine (UTM). The corrugated shear panels were painted with hydrated lime to observe the yielding regions (Fig. 2(g)).

2.2 Material properties

The material properties of the corrugated steel plate and steel UNP80 profiles were determined using the coupon tension test described in ASTM A370-22 [49]. The thicknesses of the tension coupon test specimens for the corrugated steel plate (Fig. 3(a)) and UNP80 (Fig. 3(b)) were t = 0.5 mm and t = 6 mm, respectively. Figure 3(c) and Table 2 show the obtained stress–strain curves and mechanical properties of the considered steel materials, respectively. It should be noted that the material properties in Table 2 were determined from the lowest obtained stress–strain curves.

2.3 Cyclic loading protocol

The UTM machine was used to apply a quasi-static cyclic loading protocol based on ATC-24 [50,51] in which the approximate estimated yield displacement for the considered specimens was 0.92 mm in the vertical direction. Because there is no prescribed limit on the amplitude of the two steps before yield displacement in ATC-24, two steps with six cycles and amplitudes of 25% and 50% of the calculated yield displacement were defined to ensure the recording of the specimen elastic behavior in this study. The increment in the subsequent steps was equal to the yield displacement and the number of cycles was decreased to two after the amplitude reached three times the yield displacement. Moreover, based on the results obtained from preliminary FE analyses of the specimens before the experimental test, it was anticipated that it was very unlikely that the specimens could undergo the displacements in the last three steps; therefore, the number of cycles in these steps was reduced to 1. It should be mentioned that during the test, when any significant event such as painting flaking, rivet loosening, or buckling occurred, an additional step with a half increment (i.e., Steps 8, 11, 14, and 16) was

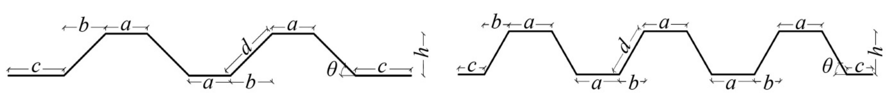

SSP-A (a) SSP-B (b)

Fig. 1 Profiles of the considered corrugated plates. (a) SSP-A; (b) SSP-B.

Table 1 Geometric properties of the experimental specimens

specimen	dimension (mm × mm)	thickness (mm)	dimensions of corrugated plate						
			no. of ridges	θ	a (mm)	h (mm)	b (mm)	c (mm)	d (mm)
SSP-A	290 × 290	0.5	2	45°	30	30	30	40	42.43
SSP-B	290 × 290	0.5	3	60°	30	30	17.3	18.04	34.63

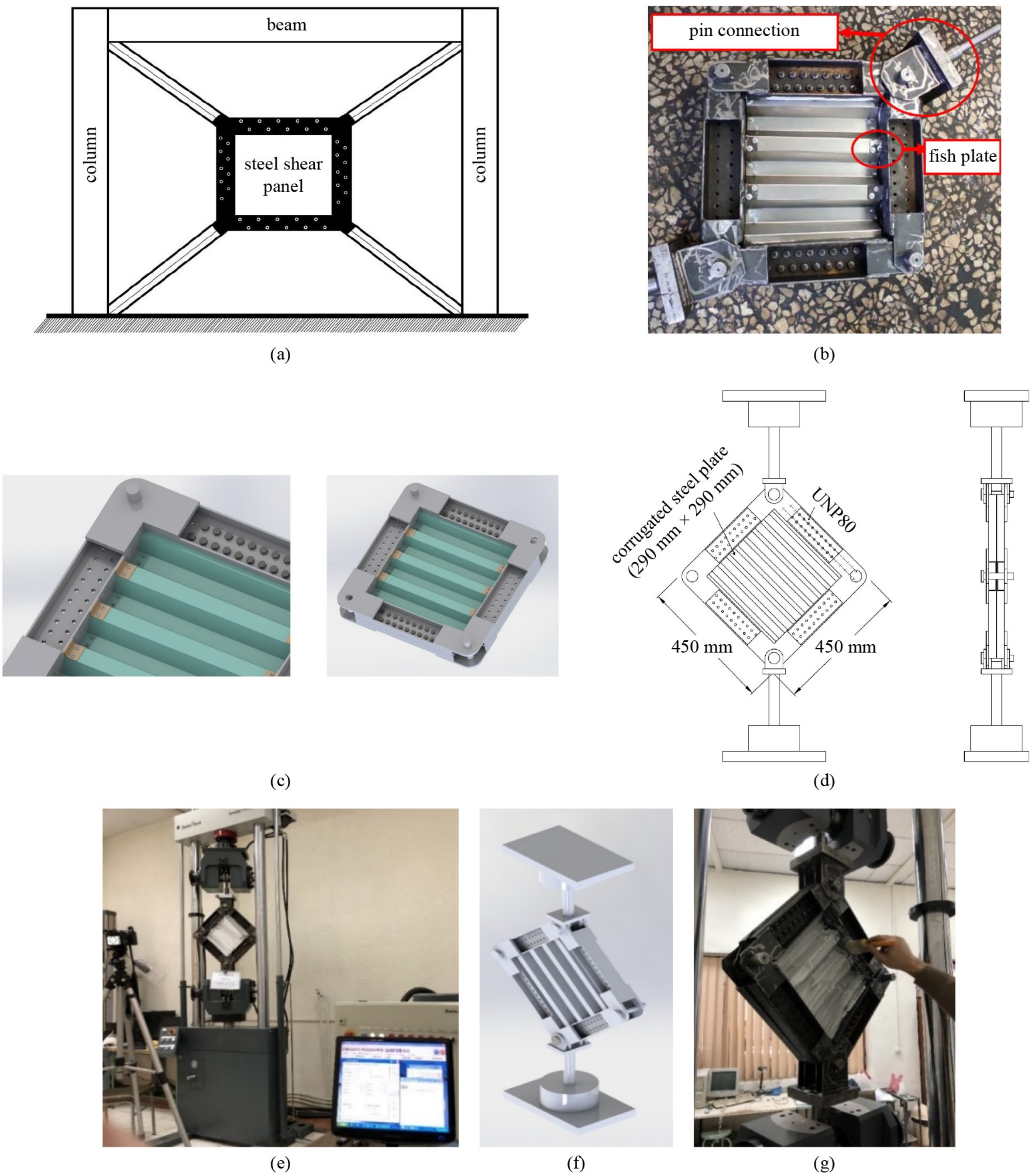

Fig. 2 (a) Schematic view of the braced steel shear panel system; (b) connection details of the shear panel to boundary elements; (c) details of the connection of the infill panel and boundary elements; (d) schematic view and geometrical dimensions of the experimental specimens; (e) the UTM experimental setup; (f) three-dimensional schematic view of the experimental setup; (g) painting of the specimens with hydrated lime.

added to the loading protocol to record any possible important events. The experimental specimens were subjected to the loading protocol along the diagonal direction to simulate the effect of the braces in braced steel shear panel systems. As shown in Table 3, this protocol involved 23 loading steps (i.e., 48 cycles) that began from an amplitude of 0.25 mm (i.e., drift of 0.056%) and ended at an amplitude of 15.75 mm (i.e., drift of 3.5%). Moreover, it should be noted that as shown in Fig. 2(a), the system in this study was a braced steel shear panel with a corrugated infill panel in which the steel shear panel was located at the center of a building frame and connected to the frame using braces. In the study by Hamed and Mofid [25], it was concluded that the optimum vertical and horizontal geometrical dimensions of the shear panel were between 10% and 30% of the story height and span length and that the shear panel should be located at the mid-point of a story.

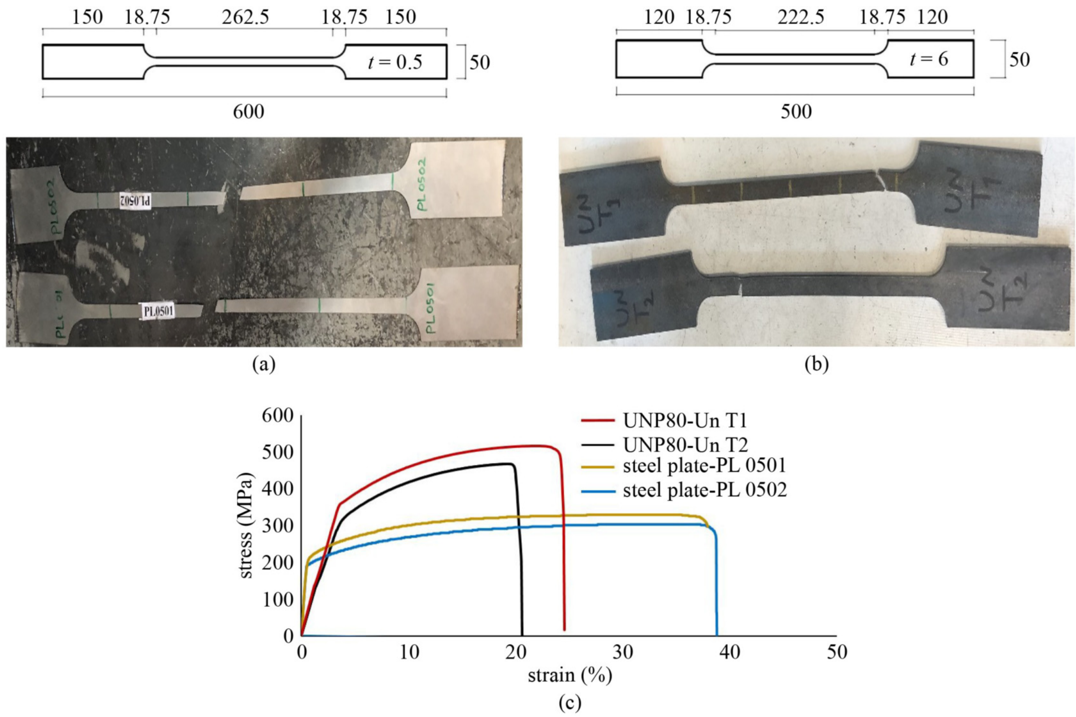

Fig. 3 Geometrical dimensions and final status of the coupon test specimens (all dimensions are in mm): (a) corrugated steel plate; (b) UNP80; (c) obtained stress–strain curves of the steel materials in the infill panel and boundary members.

Table 2 Mechanical properties of the considered steel materials

type	steel grade	elastic modulus (GPa)	yield stress (MPa)	ultimate stress (MPa)	ultimate strain (%)
corrugated steel plate	St14	205	190	303	35
UNP80	St37	203	320	468	20

Table 3 Applied loading time history protocol based on ATC-24 [51]

displacement (mm)	drift (%)	no. of cycles
0.25	0.056	3
0.46	0.102	3
0.92	0.204	3
1.84	0.409	3
2.76	0.613	3
3.68	0.818	2
4.60	1.022	2
5.06	1.124	2
5.52	1.227	2
6.44	1.431	2
6.90	1.533	2
7.36	1.636	2
8.28	1.840	2
8.74	1.942	2
9.20	2.045	2
9.66	2.147	2
10.12	2.249	2
11.04	2.454	2
11.96	2.658	2
12.88	2.863	2
13.80	3.067	1
14.72	3.272	1
15.75	3.500	1

Depending on the span length and story height of the building frame, the experimental specimens in this study, which had the dimensions of 450 mm × 450 mm, can be considered as full-scale specimens. It is therefore necessary for the early yielding of the steel shear panel to occur at very small drift ratios compared to that of the frame itself.

2.4 Discussion on experimental observations

2.4.1 Steel shear panel-A specimen

Figure 4 shows the evolution of the steel shear panel-A (SSP-A) specimen during different steps of the test. At a drift of 1% (i.e., displacement amplitude of 4.5 mm) shown in Fig. 4(a), the fish plate denoted by a red circle and the plate ridges leading to it were slightly deformed under the applied shear force and one of the rivets was loosened. Moreover, the painting began to crack and flake around the fish plates and at the corners of the corrugated plate. As shown in Fig. 4(b), the second rivet on the same fish plate was loosened at a drift of 1.4% (i.e., displacement amplitude of 6.28 mm), and painting flaking occurred around the lower fish plate. At a drift of

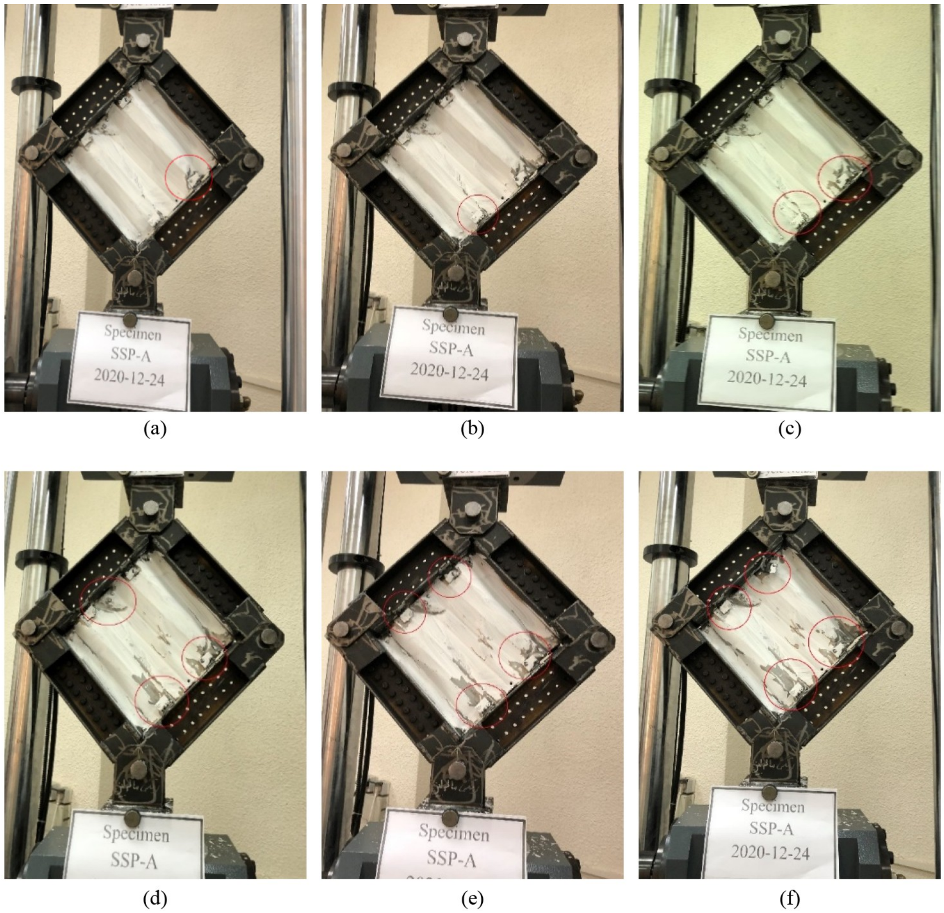

Fig. 4 Status of the SSP-A specimen during the test at the drift values of: (a) 1%; (b) 1.4%; (c) 1.86%; (d) 2.2%; (e) 2.44%; (f) 2.55%.

1.86% (i.e., displacement amplitude of 8.4 mm), the painting flaking spread to the central region of the corrugated panel (Fig. 4(c)). The painting flaking continued to develop until the end of the test and, as depicted in Fig. 4(d), began to intensify at a drift of 2.2% (i.e., displacement amplitude of 9.93 mm). At a drift of 2.44% (i.e., displacement amplitude of 11.01 mm), the amount of crumpling in the corrugated plate increased (Fig. 4(e)). As depicted in Fig. 4(f), owing to the fracture of two additional rivets, the test was stopped at a displacement amplitude of 11.51 mm (i.e., drift of 2.55%). The obtained hysteretic curve of SSP-A is shown in Fig. 5. The curve exhibits pinching owing to the buckling of the infill panel and separation of the two fish plates.

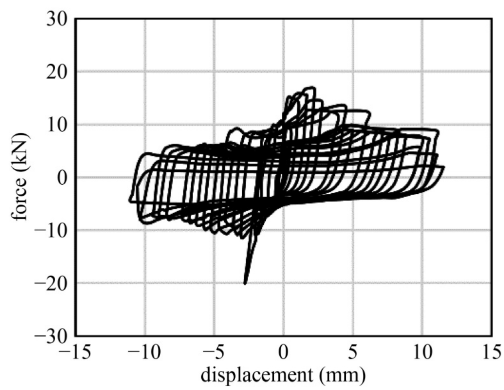

Fig. 5 Hysteretic curve of the SSP-A specimen.

2.4.2 Steel shear panel-B specimen

Figure 6 shows the evolution of the steel shear panel-B (SSP-B) specimen during different steps in the test. As shown in Fig. 6(a), the first local buckling occurred at a drift of 1.02% (i.e., displacement amplitude of 4.6 mm). The painting began to crack and flake, and cracking and flaking were clearly observed at a drift value of 1.21% (i.e., displacement amplitude of 5.43 mm) (Fig. 6(b)). At a drift value of 1.38% (i.e., displacement amplitude of 6.22 mm), another major crumpling occurred in the opposite direction (Fig. 6(c)). An additional major crumpling of the plate occurred at a drift value of 1.97% (i.e., displacement amplitude of 8.90 mm) and one of the fish plates was torn, as shown in Fig. 6(d). At the drift values of 2% and 2.07% (i.e., displacement amplitudes of 9.01 and 9.66 mm, respectively), the plate began to crumple and the painting flaking spread across the corrugated plate (Fig. 6(e)). Because of the loosening of

(a) (b) (c) (d) (e) (f)

Fig. 6 Status of the SSP-B specimen during the test at the drift values of: (a) 1.02%; (b) 1.21%; (c) 1.38%; (d) 1.97%; (e) 2%; (f) 2.07%.

an additional fish plate and a small tearing in the buckled region of the infill panel (i.e., inside the red circle on the right side of Fig. 6(f)), the test was stopped at a drift of 2.07% (Fig. 6(f)). The obtained hysteretic curve of SSP-B shown in Fig. 7 has a more stable cyclic behavior compared to that of SSP-A.

Table 4 presents the values obtained for the initial stiffness, ultimate strength, and dissipated energy of the SSP-A and SSP-B experimental specimens. The initial stiffness was calculated using the ideal bilinear curve obtained from the hysteretic curves according to FEMA 356.

As a general comparative summary of the experimental observations, it can be concluded that the only factor that resulted in the different behaviors of the two tested specimens (i.e., SSP-A and SSP-B) was the corrugation angle, which in turn affected the number of ridges. Moreover, as shown in Table 1, the other two parameters that influence the performance of the CSSPs (i.e., the sub-panel width and plate thickness) were kept constant in this experimental study. The obtained results imply that the limit state (i.e., failure mechanism) of CSSPs is a combination of tension field action development and shear yielding (Figs. 4 and 6). However, at small plate thicknesses (e.g., t = 0.5 mm) and corrugation angles, the tension field action limit state was dominant. As a result, SSP-A exhibited more buckling, which resulted in further pinching in its hysteretic curve (Fig. 5). In addition, comparing the performance of the corrugations to that of the braces in the building frames, it can be seen from

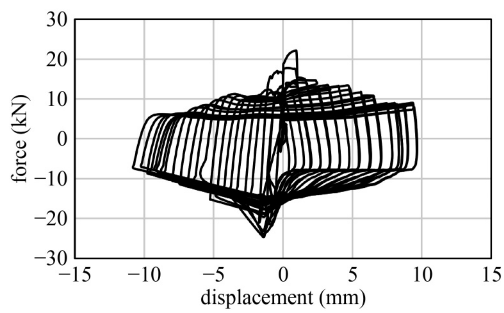

Fig. 7 Hysteretic curve of the SSP-B specimen.

Table 4 Comparison of the obtained experimental results for the SSP-A and SSP-B specimens

specimen	initial stiffness (kN/mm)	dissipated energy (kN·m)	ultimate strength (kN)
SSP-A	34.62	2.39	21.38
SSP-B	19.97	5.8	23.16

Table 4 that as the corrugation angle increased, the degree of its effect on the lateral stiffness of the panels decreased, and as a result, the initial stiffness of SSP-B decreased. However, owing to its more stable hysteretic behavior (Fig. 7), SSP-B had a higher ultimate strength and energy dissipation. Moreover, it is possible that the infill panel may be torn owing to stress concentration at sharp angles (e.g., corrugation angle of 90°) or the low-cycle fatigue of the infill panel at the intersection of the buckled regions as a result of periodic changes in the loading direction and subsequent frequent crumpling of the plate. In the specimens tested in this study, one of the SSP-B fish plates (Fig. 6(d)) was torn and a very small tear was observed at the buckled region inside the red circle on the right side of Fig. 6(f), which can probably be attributed to fatigue. Owing to the importance of fatigue in the cyclic behavior of CSSWs, this issue should be investigated in detail in future research.

3 Verification of finite element modeling

The FE model is presented in this section and its validity and accuracy evaluated. The FE models were fitted to the SSP-A and SSP-B specimens tested in this study to verify the FE modeling procedure. The S4R element (ABAQUS) was used for all the components of the models. The coupling interaction was used at the four corners of the shear panel model to simulate the pinned connection of the boundary elements such that all degrees of freedom, except for in-plane rotation, were constrained. The steel material properties were defined based on the stress–strain curves presented in Subsection 2.2 and kinematic hardening was assigned. The models were subjected to the considered quasistatic loading (Table 3) using a general static analysis step. There is good agreement between the experimental and numerical hysteretic curves (Figs. 8(a) and 8(b)) and the final deformation shapes (Figs. 8(c) and 8(d)). The FE model and experimental values of the ultimate strength and dissipated energy are compared in Table 5. The coincidence of the hysteretic curves and the proximity of the $F_{\mathrm{num}}/F_{\mathrm{exp}}$ and $E_{\mathrm{num}}/E_{\mathrm{exp}}$ values to 1 indicate the acceptable accuracy of the FE modeling where F_{num}, F_{exp}, E_{num}, and E_{exp} represent the ultimate strengths and dissipated energies in the FE models and experimental specimens, respectively. The agreement between the experimental data and numerical results indicates that the FE models can be confidently employed in the parametric study.

4 Parametric study

In this section, nonlinear static analyses are performed to assess the effects of the subpanel width (a), corrugation angle (θ), and panel thickness (t) on the CSSP performance. Table 6 shows the specifications of the considered models, which were modeled using the verified modeling procedure and material properties described in Section 3 and Subsection 2.2, respectively.

4.1 Sub-panel width

The effect of the subpanel width was studied for three different sizes. As shown in Fig. 9, the subpanel size had a notable effect on the postbuckling behavior of the panel. A sudden spike occurred in the shear force–displacement curves of the panels as the subpanel size increased. Moreover, from the presented values for the initial stiffness, ultimate strength, and energy dissipation capacity of the CSSPs, it is seen that as the sub-panel width increased, the probability of panel buckling increased, and the behavior of the CSSP tended to that of an unstiffened shear panel. The CSSP stiffness and strength therefore decreased (Table 7).

4.2 Corrugation angle

Five different corrugation angles (15°, 30°, 45°, 60°, and 90°) were used in the parametric study. The shear force–displacement curves in Fig. 10 show that the CSSP with a corrugation angle of 15° was ductile and exhibited no sudden reduction in its strength. However, increasing the corrugation angle caused a sudden reduction in the shear force. The results in Table 8 show that as the corrugation angle increased, the ultimate strength and dissipated energy generally increased while the initial stiffness decreased. By comparing the performance of the inclined parts of subpanels to braces with different angles (e.g., concentrically braced frames), it can be concluded that the stiffness decreased as the angle increased to 90°. In addition, excessive reductions of the corrugation angle caused the shear wall behavior to become closer to that of unstiffened shear walls with lower stiffness. It is also noteworthy that strength recovery (i.e., restoration) occurred in the obtained shear force–displacement curves for the θ values of 15° and 30° but disappeared at higher values of θ. It should be mentioned that as the corrugation angle decreased, the behavior of the CSSP tended toward that of an unstiffened shear panel in which the postbuckling strength resulted from the development of the tension field action. This phenomenon was not observed for corrugation angles of 45° and above. This conclusion is confirmed by the experimental results obtained in this study (Figs. 5 and 7).

4.3 Plate thickness

The effects of the plate thickness on the performance of the CSSP are presented in this section. The plate thickness values of 0.5, 1.25, and 2 mm were considered for this purpose. From the obtained results (Fig. 11 and

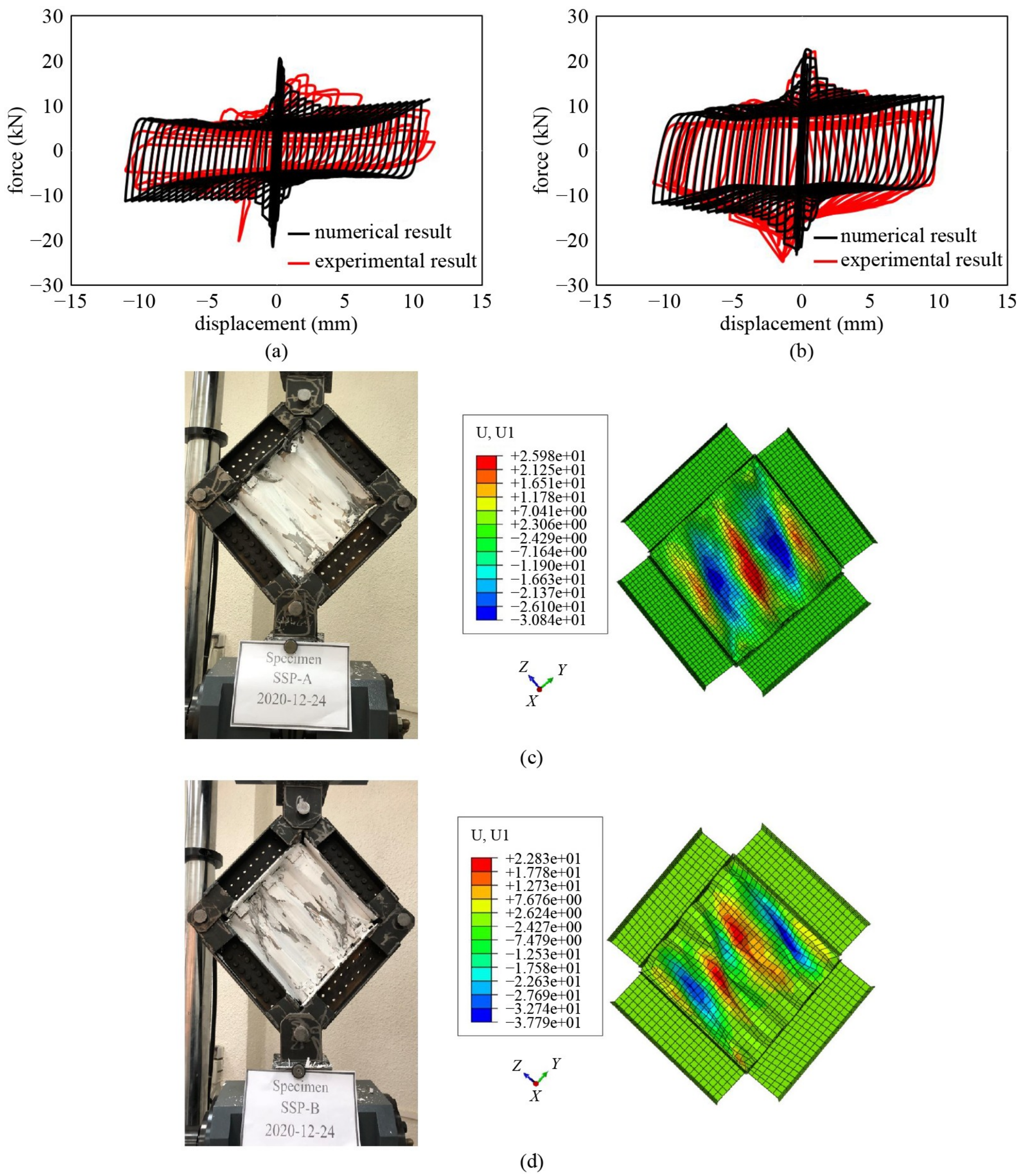

Fig. 8 Comparison of the obtained hysteresis force–displacement curves for experimental specimens (black line) and FE models (red line): (a) SSP-A; (b) SSP-B; comparison of the final experimental and numerical deformed shapes of (c) SSP-A and (d) SSP-B.

Table 5 Comparison of the obtained values from the FE models and experimental specimens

specimen	ultimate strength (kN)			dissipated energy (kN·m)		
	F_{exp}	F_{num}	F_{num}/F_{exp}	E_{exp}	E_{num}	E_{num}/E_{exp}
SSP-A	21.38	20.07	0.938	2.39	2.92	1.22
SSP-B	23.16	24.63	1.06	5.8	5.28	0.91

Table 9), it can be concluded that increasing the thickness of the panel increased its initial stiffness, dissipated energy capacity, and ultimate strength. In general, the results obtained for the corrugation angle sensitivity analysis in Subsection 4.2 and plate thickness parametric analysis in Subsection 4.3 indicate that plate buckling inevitably occurred at every corrugation angle in CSSPs with small plate thicknesses, even in the combined limit state (i.e., tension field action and shear yielding) that

Table 6 Specifications of the studied FE models

a (mm)	t (mm)	$\theta = 15°$	$\theta = 30°$	$\theta = 45°$	$\theta = 60°$	$\theta = 90°$
30	0.5	A	C	E	G	I
	1.25	AA	BB	CC	DD	EE
	2	B	D	F	H	J
60	0.5	–	K	M	O	Q
	1.25	–	FF	GG	HH	II
	2	–	L	N	P	R
90	0.5	–	S	U	W	Y
	1.25	–	JJ	KK	LL	MM
	2	–	T	V	X	Z

occurred at higher corrugation angles. Moreover, as the corrugation angle decreased, the CSSP performance tended to that of the unstiffened SPSWs, in which the governing limit state was tension field development. The

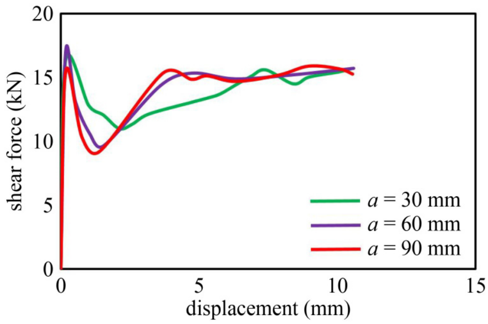

Fig. 9 Force–displacement curves of CSSP models with different sub-panel widths ($\theta = 30°$ and $t = 0.5$ mm).

Table 7 Comparison of obtained results for CSSP models with different sub-panel widths

sub-panel width (mm)	initial stiffness (kN/mm)	ultimate strength (kN)	dissipated energy (kN·m)
30	95.5	16.3	0.142
60	96.7	17	0.148
90	88.8	15.92	0.148

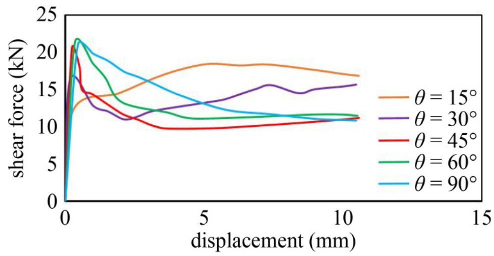

Fig. 10 Force–displacement curves for CSSP models with different corrugation angles ($a = 30$ mm and $t = 0.5$ mm).

Table 8 Comparison of obtained results for CSSP models with different corrugation angles

corrugation angle (°)	initial stiffness (kN/mm)	ultimate strength (kN)	dissipated energy (kN·m)
15	40.4	18.46	0.117
30	95.5	16.3	0.142
45	85.65	20.6	0.117
60	60.5	21.38	0.132
90	46.22	21.12	0.145

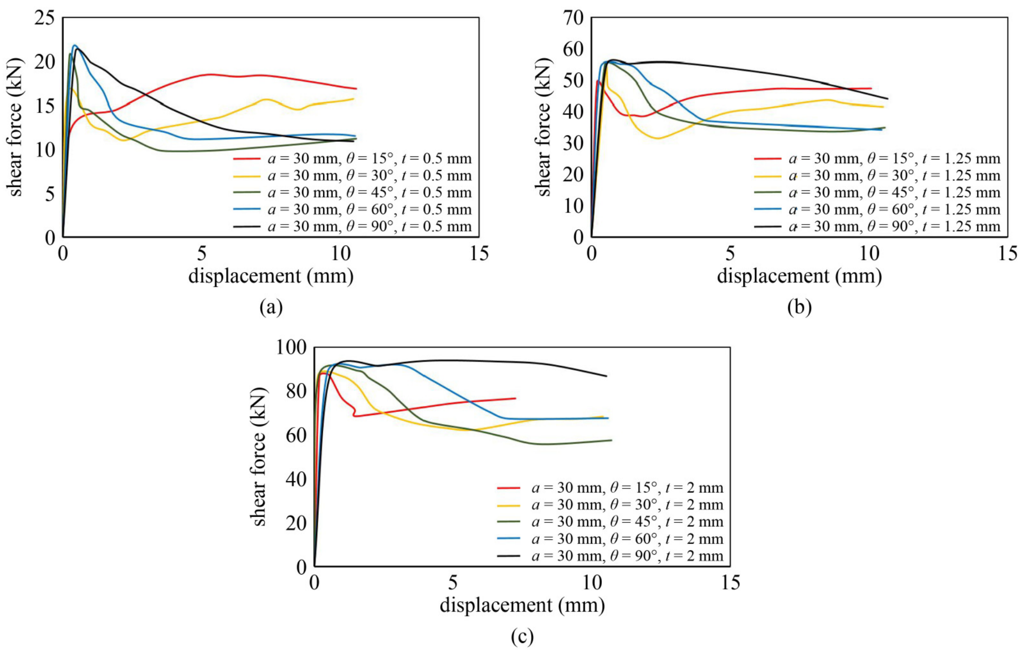

Fig. 11 Force–displacement curves of CSSP models with different plate thicknesses and corrugation angles ($a = 30$ mm): (a) $t = 0.5$ mm; (b) $t = 1.25$ mm; (c) $t = 2$ mm.

Table 9 Comparison of obtained results for CSSP models with different plate thicknesses ($a = 30$ mm)

θ (°)	dissipated energy (kN·m)			initial stiffness (kN/mm)			ultimate strength (kN)		
	$t = 0.5$ mm	$t = 1.25$ mm	$t = 2$ mm	$t = 0.5$ mm	$t = 1.25$ mm	$t = 2$ mm	$t = 0.5$ mm	$t = 1.25$ mm	$t = 2$ mm
15	0.174	0.462	0.773	40.4	243	470	18.46	49.57	87.53
30	0.142	0.411	0.717	95.5	103.5	697.5	16.75	54.44	87.55
45	0.117	0.393	0.719	85.6	113.5	518.2	20.89	54.83	89.98
60	0.132	0.416	0.808	60.5	164.7	187.7	21.73	55.09	92.03
90	0.144	0.539	0.937	46.22	102.13	148.45	21.40	55.57	93.85

CSSPs with medium and large plate thicknesses exhibited a decreased amount of buckling and were governed by the shear yielding limit state. Less buckling occurred as the corrugation angle increased. It is known that the complete development of tension field action or complete net shear yielding results in more ductile behavior; therefore, as shown in Fig. 11, at small and large plate thicknesses, more ductile behavior was exhibited at the corrugation angles of 15° and 90°, respectively, and there was no sudden reduction in the strength of the panel. Moreover, the amount of crumpling on the panel decreased as the panel thickness increased.

4.4 Optimal corrugated steel shear panel model

The CSSP with the best performance among the 39 studied models in terms of the obtained hysteretic curves and parameters is selected in this section. From Fig. 12,

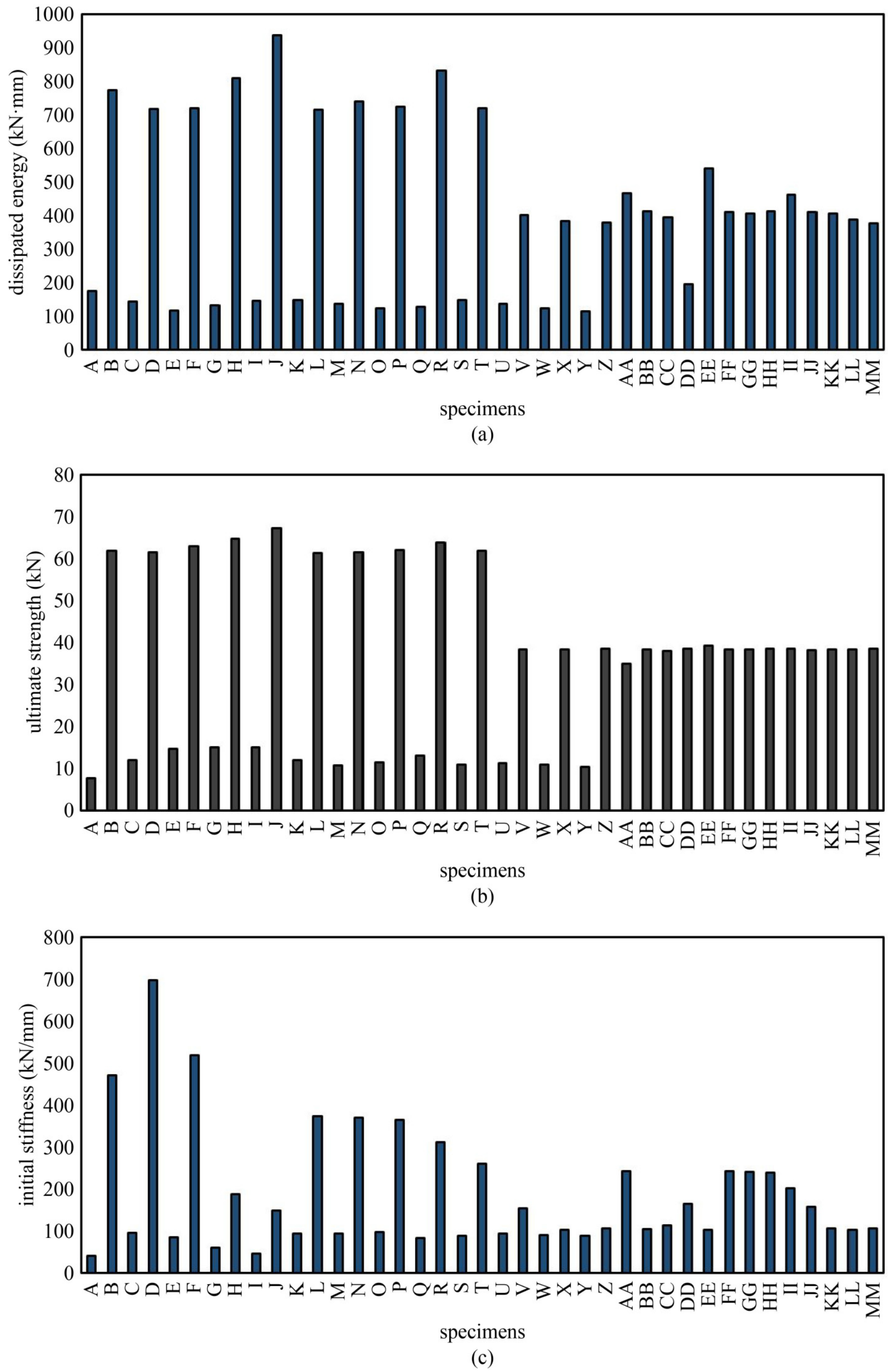

Fig. 12 Variation of the calculated parameters in the studied FE models: (a) dissipated energy; (b) ultimate strength; (c) initial stiffness.

which shows the values of the calculated parameters for all the models, it is concluded that model J (i.e., a = 30 mm, t = 2 mm, θ = 90°) has the highest energy dissipation capacity and ultimate strength, whereas model D (i.e., a = 30 mm, t = 2 mm, θ = 30°) has the highest initial stiffness. Meanwhile, the results indicate that the models with t = 0.5 and 1.25 mm have a uniform energy dissipation capacity and ultimate strength.

5 Estimation of buckling shear strength

A closed-form equation for estimating the buckling shear strength of CSSPs from their geometrical parameters is presented in this section. The buckling shear strengths of all the considered models (Table 6) were obtained through the following process.

1) Buckling analysis was performed to determine the critical buckling mode (Fig. 13).

2) The time step of the buckled panel that matches the critical buckling mode was identified.

3) The equivalent displacement was determined from the time step of the buckled panel and the buckling load specified from the hysteretic curve.

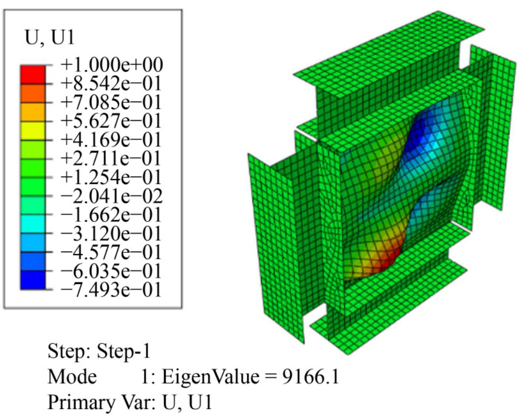

Fig. 13 Buckling analysis to control the CSSP shear strength.

4) The shear strength of the panel was calculated by applying a force along the diagonal direction of the panel using the projection of the buckling load to 45°.

This process was performed for all the studied models and the shear strengths for different parameters determined. Figure 14 shows the variation of the shear strength with the two parameters θ and t/a. The relationship between the shear strength and the considered parameters (Eq. (1)) was extracted using surface regression as

$$T_{cr} = 363.7 + 1.754\times10^6\left(\frac{t}{a}\right) + 34.21\theta - 1.378\times10^7\left(\frac{t}{a}\right)^2 + 1050\left(\frac{t}{a}\right)\theta, \quad (1)$$

where t, a, and θ are the plate thickness, subpanel width, and corrugation angle of the steel panel, respectively. The shear strengths obtained from the experimental and numerical CSSPs are presented in Table 10 and compared with the values estimated using Eq. (1). It can be seen that the average percentage deviation is 15%, which is an acceptable accuracy.

6 Conclusions

In this study, the structural performance of CSSPs was

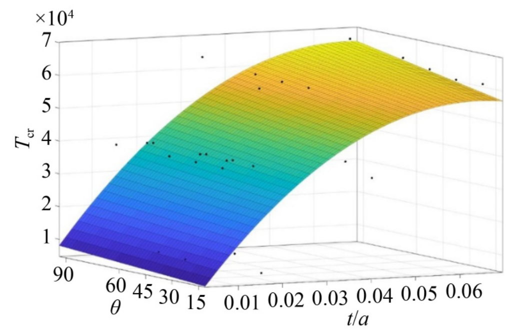

Fig. 14 Surface regression of CSSP shear strength.

Table 10 Comparison of the CSSP shear strengths obtained from the experiment, numerical calculations, and Eq. (1)

specimen	a (mm)	t (mm)	t/a	θ (°)	experimental/numerical result	Eq. (1)	percentage difference (%)
SSP-A	30	0.5	0.017	45	15117.9	17352.1	14.79
SSP-B	30	0.5	0.017	60	16376.6	19075.9	16.48
B	30	2	0.067	15	61894.5	57349.07	13.81
FF	30	1.25	0.042	60	38545.1	44034.35	11.70
JJ	30	1.25	0.042	90	39193.1	44542.71	13.65
JJ	45	0.5	0.011	90	11372.3	11462.563	15.03
P	60	2	0.033	60	62019.4	57538.522	7.23
K	60	0.5	0.008	30	12045.1	13278.888	16.05
W	90	0.5	0.006	60	10853.2	9563.213	11.89
S	90	0.5	0.006	30	10855.2	9061.913	16.53

investigated. For this purpose, two experimental specimens were constructed and their behavior was investigated using a quasi-static cyclic loading time history. After validating the FE modeling procedure, a parametric study was performed to investigate the effects of geometrical properties such as the corrugation angle, sub-panel width, and plate thickness on the CSSP performance. Finally, a closed-form relationship to estimate the buckling shear strength of the CSSPs without considering residual stresses was presented. It should be mentioned that the findings of a comparative study by the authors on the effects of the residual stresses generated during the forming process (i.e., pressing) of the steel panel will be presented in the near future. The main results of this study are as follows.

1) Increasing the number of ridges and grooves (i.e., corrugation) resulted in more stable hysteretic curves, which increased the energy dissipation capacity.

2) As the sub-panel width increased, the probability of panel buckling increased and the behavior of the CSSP tended toward that of the unstiffened shear panels. The CSSP stiffness and strength therefore decreased. In addition, the shear force–displacement curves of CSSPs with smaller sub-panel widths exhibited more stable behavior.

3) The ultimate strength and dissipated energy capacity of the CSSPs increased while the initial stiffness decreased as the corrugation angle of the panel increased from 15° to 90°.

4) Increasing the plate thickness increased the initial stiffness, dissipated energy capacity, and ultimate strength of the CSSPs.

5) The CSSP with a = 30 mm, t = 2 mm, and θ = 90° has the highest energy dissipation capacity and ultimate strength while the CSSP with a = 30 mm, t = 2 mm, and θ = 30° has the highest initial stiffness. It can be concluded that the latter CSSP has the best structural performance.

6) An equation to estimate the buckling shear strength of CSSPs was proposed.

7) It should be mentioned that buckling and pinching of the hysteretic curve are always observed in the cyclic behavior of SPSWs. Different solutions such as the use of stiffened SPSWs, ring-shaped SPSWs, SPSWs with buckling-restrained plates, auxetic-shaped SPSWs, and SPSWs with optimized configurations have been introduced to address the infill panel buckling issue and increase the stability of the obtained hysteretic curve. One solution is the use of corrugated SPSWs, which was discussed in this study. Although some of the previously proposed dampers have more stable hysteretic curves compared to that of the CSSP, the focus of this study is on investigating the cyclic performance of unstiffened SPSWs and providing a solution to enhance their cyclic performance so that the solution can be used as a safe and reliable alternative to unstiffened SPSWs. More stable hysteretic curves for unstiffened SPSWs were achieved in the considered experimental specimens, particularly for the SSP-B specimen. According to the results in this study and as mentioned in the previous sections, a combined limit state of tension field action development and shear yielding occurred in the CSSPs; hence, buckling occurred even in CSSPs, especially in CSSPs with smaller plate thicknesses. It can therefore be concluded that buckling is one of the limitations of this type of metallic yielding dampers and that future research should continue to focus on this issue.

References

1. Fang C, Wang W, Qiu C, Hu S, MacRae G A, Eatherton M R. Seismic resilient steel structures: A review of research, practice, challenges and opportunities. Journal of Constructional Steel Research, 2022, 191: 107172
2. Alinia M, Dastfan M. Behaviour of thin steel plate shear walls regarding frame members. Journal of Constructional Steel Research, 2006, 62(7): 730−738
3. Takahashi Y, Takemoto Y, Takeda T, Takagi M. Experimental study on thin steel shear walls and particular bracings under alternative horizontal load. In: Symposium on Resistance and Ultimate Deformability of T sructures Acted on by Well-defined Repeated Loads. Lisbon: IABSE, 1973
4. Pirmoz A. Beam-attached steel plate shear walls. Structural Design of Tall and Special Buildings, 2012, 21(12): 879−895
5. Xue M, Lu L. Interaction of infilled steel shear wall panels with surrounding frame members. In: Proceedings of the Structural Stability Research Council Annual Technical Session. Bethlehem, PA: SSRC, 1969
6. Neal J, Qu B. Steel plate shear walls with controlled infill tension fields. In: Structures Congress 2011. Las Vegas, NV: ASCE, 2011
7. Emamyari A, Sheidaii M R, Kookalanifar A, Showkati H, Akbarzadeh N. Experimental study on cyclic behavior of stiffened perforated steel shear panels. Structures, 2020, 27: 2400−2410
8. Formisano A, Lombardi L, Mazzolani F. Perforated metal shear panels as bracing devices of seismic-resistant structures. Journal of Constructional Steel Research, 2016, 126: 37−49
9. Monsef Ahmad H, Sheidaii M R, Tariverdilo S, Formisano A, de Matteis G. Experimental and numerical study of perforated steel plate shear panels. International Journal of Engineering, 2020, 33(4): 520−529
10. Roberts T M, Sabouri-Ghomi S. Hysteretic characteristics of unstiffened perforated steel plate shear panels. Thin-walled Structures, 1992, 14(2): 139−151
11. Vian D. Steel plate shear walls for seismic design and retrofit of building structures. Dissertation for the Doctoral Degree. Buffalo, NY: State University of New York at Buffalo, 2005
12. Vian D, Bruneau M. Testing of special LYS steel plate shear walls. In: Proceedings of the 13th World Conference on Earthquake Engineering. Vancouver: 13 WCEE Secretariat, 2004

13. Vian D, Bruneau M, Purba R. Special perforated steel plate shear walls with reduced beam section anchor beams. II: Analysis and design recommendations. Journal of Structural Engineering, 2009, 135(3): 221−228
14. Vian D, Bruneau M, Tsai K C, Lin Y C. Special perforated steel plate shear walls with reduced beam section anchor beams. I: Experimental investigation. Journal of Structural Engineering, 2009, 135(3): 211−220
15. De Matteis G, Brando G, Mazzolani F M. Pure aluminium: An innovative material for structural applications in seismic engineering. Construction & Building Materials, 2012, 26(1): 677−686
16. de Matteis G, Mazzolani F M, Panico S. Seismic protection of steel buildings by pure aluminium shear panels. In: Proceeding of 13th World Conference on Earthquake Engineering. Vancouver: 13 WCEE Secretariat, 2004
17. Nakagawa S, Kihara H, Torii S, Nakata Y, Matsuoka Y, Fujisawa K, Fukuda K. Hysteretic behavior of low yield strength steel panel shear walls: Experimental investigation. In: Proceedings of the 11th WCEE. Oxford: Elsevier, 1996, 171
18. Soltani N, Abedi K, Poursha M, Golabi H. An investigation of seismic parameters of low yield strength steel plate shear walls. Earthquakes and Structures, 2017, 12(6): 713−723
19. Hitaka T, Matsui C. Experimental study on steel shear wall with slits. Journal of Structural Engineering, 2003, 129(5): 586−595
20. Kurata M, Leon R T, DesRoches R, Nakashima M. Steel plate shear wall with tension-bracing for seismic rehabilitation of steel frames. Journal of Constructional Steel Research, 2012, 71: 92−103
21. Akbari Hamed A, Mofid M. On the plastic analysis of concentrically braced frames with shear panel, obtaining predetermined collapse mechanism. Structural Design of Tall and Special Buildings, 2015, 24(5): 366−395
22. Akbari Hamed A, Mofid M. On the experimental and numerical study of braced steel shear panels. Structural Design of Tall and Special Buildings, 2015, 24(14): 853−872
23. Akbari Hamed A, Mofid M. Plastic design of eccentrically braced frames with shear panels. Proceedings of the Institution of Civil Engineers—Structures and Buildings, 2017, 170(1): 17−32
24. Hamed A A, Mofid M. On the equivalent simple models of braced steel shear panels. Proceedings of the Institution of Civil Engineers—Structures and Buildings, 2015, 168(8): 570−577
25. Hamed A A, Mofid M. Parametric study and computation of seismic performance factors of braced shear panels. Scientia Iranica, 2016, 23(2): 460−474
26. Khazaei-Poul M, Nateghi-Alahi F, Alavi E. Seismic behaviour of concentrically braced frame system combined with steel shear panel. In: Proceedings of the 9th International Congress on Civil Engineering. Isfahan: Isfahan University of Technology, 2012
27. Hamed A A, Asl R B, Rahimzadeh H. Experimental and numerical study on the structural performance of auxetic-shaped, ring-shaped and unstiffened steel plate shear walls. Journal of Building Engineering, 2021, 34: 101939
28. Hamed A A, Samadi A, Basim M C. Topology and shape optimization of steel plate shear walls for enhancing the seismic energy dissipation capacity. Journal of Building Engineering, 2022, 57: 104828
29. Berman J. Moveable Infills for Seismic Energy Dissipation. Student Research Accomplishments. Buffalo, NY: University at Buffalo, 2001
30. Emami F, Mofid M, Vafai A. Experimental study on cyclic behavior of trapezoidally corrugated steel shear walls. Engineering Structures, 2013, 48: 750−762
31. Yadollahi Y, Pakar I, Bayat M. Evaluation and comparison of behavior of corrugated steel plate shear walls. Latin American Journal of Solids and Structures, 2015, 12(4): 763−786
32. Hosseinpour E, Baharom E S, Yadollahi Y. Evaluation of steel shear walls behavior with sinusoidal and trapezoidal corrugated plates. Advances in Civil Engineering, 2015, 1−11
33. Farzampour A, Laman J A, Mofid M. Behavior prediction of corrugated steel plate shear walls with openings. Journal of Constructional Steel Research, 2015, 114: 258−268
34. Bahrebar M, Kabir M Z, Hajsadeghi M, Zirakian T, Lim J B P. Structural performance of steel plate shear walls with trapezoidal corrugations and centrally-placed square perforations. International Journal of Steel Structures, 2016, 16(3): 845−855
35. Zheng L, Wang W, Ge H, Guo H, Gao Y, Han Y. Seismic performance of steel corrugated plate structural walls with different corrugation inclinations. Journal of Constructional Steel Research, 2022, 192: 107248
36. Roudsari S S, Soleimani S M, Hamoush S A. Analytical study of the effects of opening characteristics and plate thickness on the performance of sinusoidal and trapezoidal corrugated steel plate shear walls. Journal of Constructional Steel Research, 2021, 182: 106660
37. Banazadeh A, Maleki A. Numerical investigation of the seismic behavior of corrugated steel shear wall by ABAQUS software. International Journal of Advanced Biotechnology and Research, 2016, 7: 608−614
38. Dou C, Jiang Z Q, Pi Y L, Guo Y L. Elastic shear buckling of sinusoidally corrugated steel plate shear wall. Engineering Structures, 2016, 121: 136−146
39. Cao Q, Huang J. Experimental study and numerical simulation of corrugated steel plate shear walls subjected to cyclic loads. Thin-walled Structures, 2018, 127: 306−317
40. Dou C, Pi Y L, Gao W. Shear resistance and post-buckling behavior of corrugated panels in steel plate shear walls. Thin-walled Structures, 2018, 131: 816−826
41. Tong J Z, Guo Y L. Shear resistance of stiffened steel corrugated shear walls. Thin-walled Structures, 2018, 127: 76−89
42. Feng L, Sun T, Ou J. Elastic buckling analysis of steel-strip-stiffened trapezoidal corrugated steel plate shear walls. Journal of Constructional Steel Research, 2021, 184: 106833
43. Tong J Z, Guo Y L, Zuo J Q. Elastic buckling and load-resistant behaviors of double-corrugated-plate shear walls under pure in-plane shear loads. Thin-walled Structures, 2018, 130: 593−612
44. Tong J Z, Guo Y L, Zuo J Q, Gao J K. Experimental and numerical study on shear resistant behavior of double-corrugated-plate shear walls. Thin-walled Structures, 2020, 147: 106485
45. Tong J Z, Guo Y L, Pan W H. Ultimate shear resistance and post-ultimate behavior of double-corrugated-plate shear walls. Journal of Constructional Steel Research, 2020, 165: 105895

46. Ghodratian-Kashan S, Maleki S. Experimental investigation of double corrugated steel plate shear walls. Journal of Constructional Steel Research, 2022, 190: 107138
47. Bahrebar M, Lim J B, Clifton G C, Zirakian T, Shahmohammadi A, Hajsadeghi M. Perforated steel plate shear walls with curved corrugated webs under cyclic loading. Structures, 2020, 24: 600−609
48. Yu Y, Hu C, Zhao F, Jiang L. Research on the specially-shaped corrugated steel plate shear walls with horizontal corrugation. Journal of Constructional Steel Research, 2022, 188: 107012
49. ASTM A370-22. Standard Test Methods and Definitions for Mechanical Testing of Steel Products. West Conshohocken, PA: ASTM, 2003
50. Fang C, Ping Y, Chen Y. Loading protocols for experimental seismic qualification of members in conventional and emerging steel frames. Earthquake Engineering & Structural Dynamics, 2020, 49(2): 155−174
51. Krawinkler H. Guidelines for Cyclic Seismic Testing of Components of Steel Structures. Redwood City, CA: Applied Technology Council, 1992